Electronic Supplementary Information for:

Structural modulation of the photophysical and electronic properties of pyrene-based 3D metal–organic frameworks derived from s-block metals

Christopher N. Coleman, Patrick C. Tapping, Michael T. Huxley, Tak W. Kee, David M. Huang*, Christian J. Doonan* and Christopher J. Sumby*

Department of Chemistry and Centre for Advanced Nanomaterials, The University of Adelaide, Adelaide, South Australia 5005, Australia.

email: christian.doonan@adelaide.edu.au, christopher.sumby@adelaide.edu.au; david.huang@adelaide.edu.au

Contents

1. MOF synthesis and characterisation

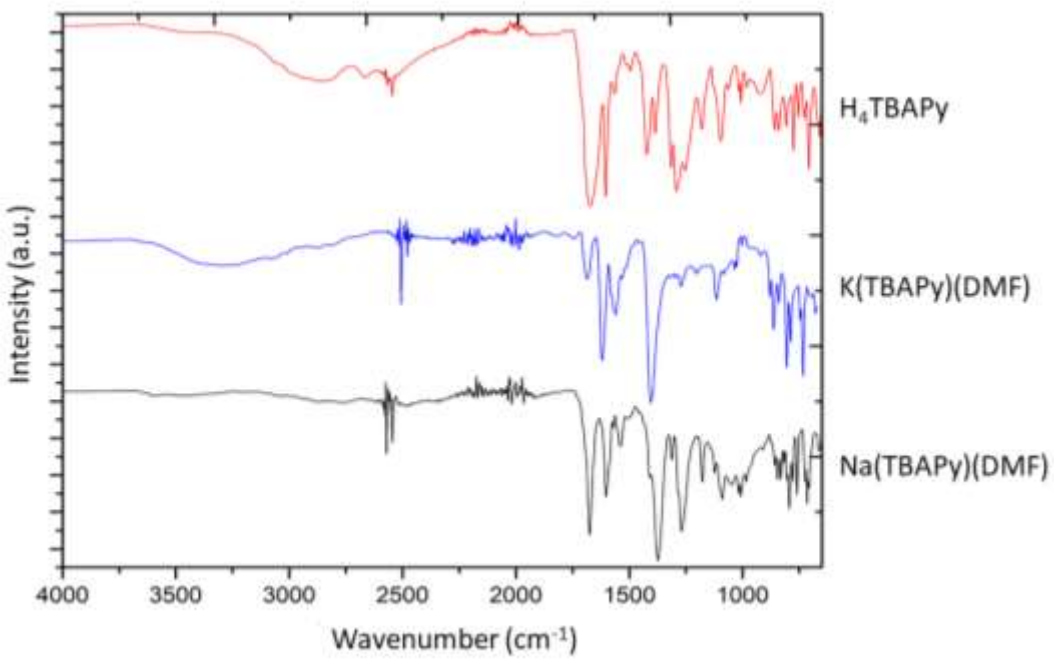

Fig. S1. Fourier-transform infrared (FTIR) spectroscopy. IR spectra of the free linker TBAPy (red), K(TBAPy)(DMF) (blue) and Na(TBAPy)(DMF) (black). Spectra were obtained on a PerkinElmer Spectrum 100 FTIR spectrometer using approximately 0.5 mg of ground sample.

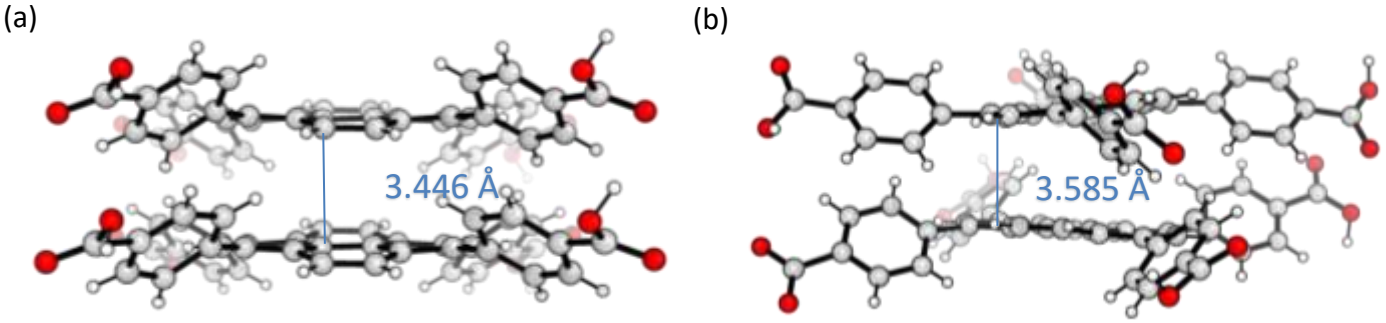

Fig. S2. Perspective views of the distinct dimers obtained from single crystal X-ray structures in (a) K(TBAPy)(DMF) and (b) Na(TBAPy)(DMF) showing the respective distances in ångstroms (Å) between the two closest ligands. The distance stated is for the two closest carbon atoms located on adjacent pyrene moieties (not centroid to centroid).

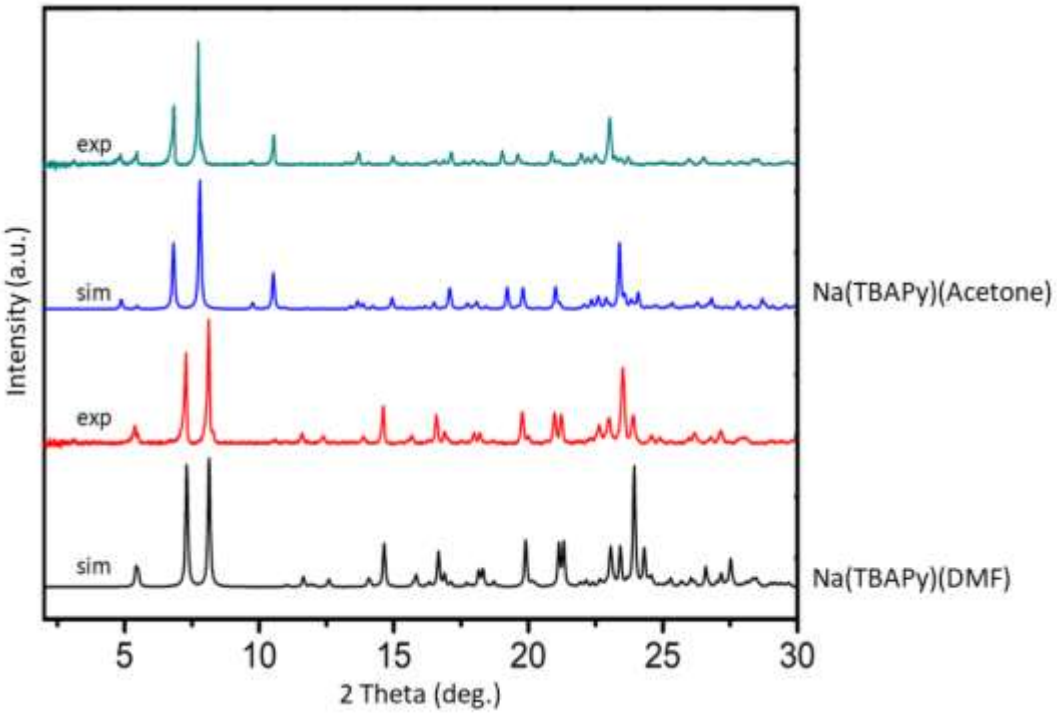

Fig. S3. Powder X-ray diffraction (PXRD) data for the sodium-based MOFs, Na(TBAPy)(acetone) and Na(TBAPy)(DMF). Single crystals of Na(TBAPy)(DMF) were obtained by soaking crystals of Na(TBAPy)(acetone) in DMF, which causes a phase change (details shown in Fig. S4).

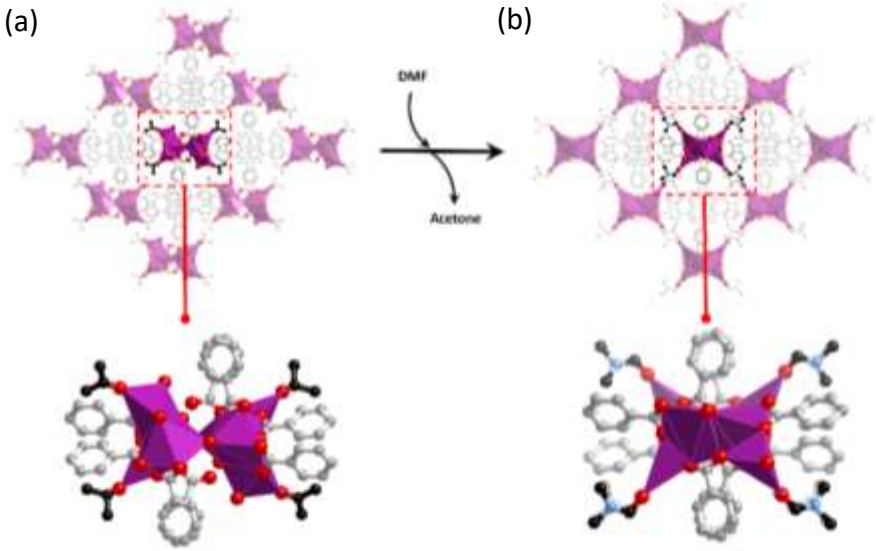

Fig. S4. The overall structure and the coordination environment around the rod-like secondary building unit of (a) Na(TBAPy)(acetone) and (b) Na(TBAPy)(DMF). Single crystals of Na(TBAPy)(DMF) were obtained by soaking crystals of Na(TBAPy)(acetone) in DMF.

(a) 

(b) 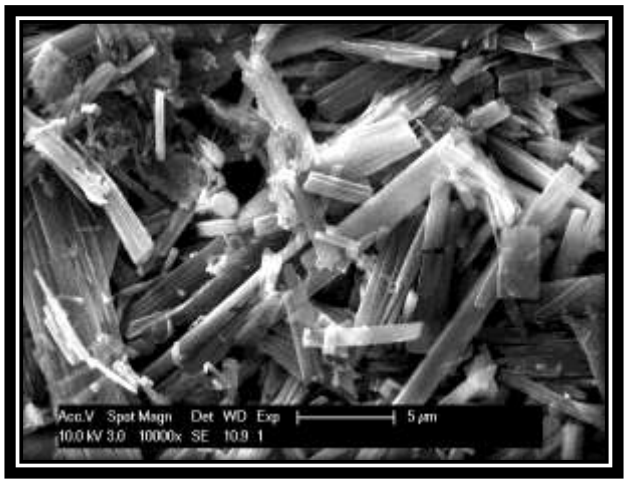

Fig. S5. Scanning electron micrograph (SEM) of microcrystalline (a) Na(TBAPy)(DMF) and (b) K(TBAPy)(DMF). SEM images were collected using a Philips XL30 field-emission scanning electron microscope (FESEM).

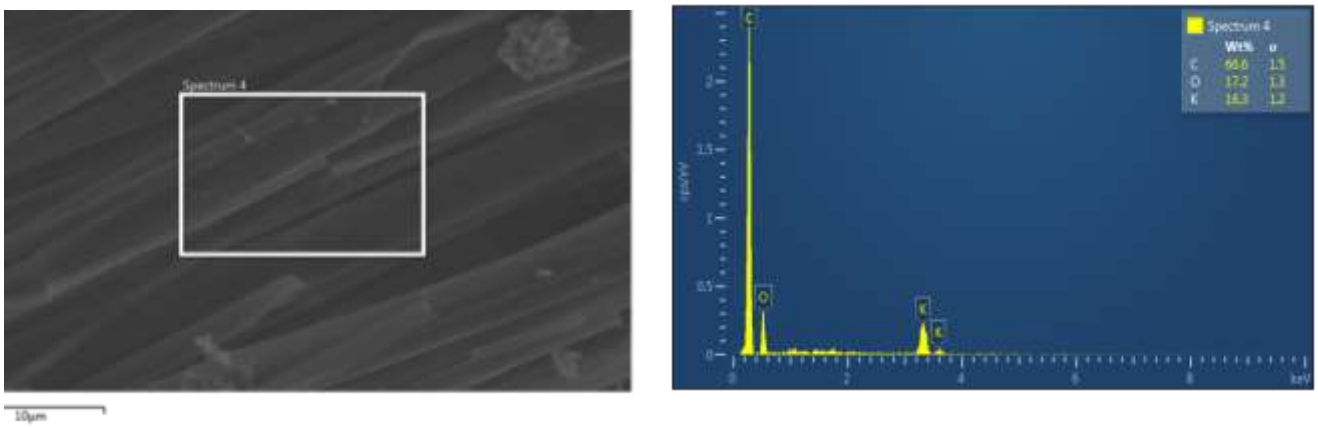

Fig. S6. Energy-dispersive X-ray (EDX) spectrum (right) taken from the identified area in the SEM image (right) of K(TBAPy)(DMF) indicating the primary components of the MOF as being K, C and O. Energy-dispersive X-ray spectroscopy (EDX) was performed on a Philips XL30 field emission scanning electron microscope**.**

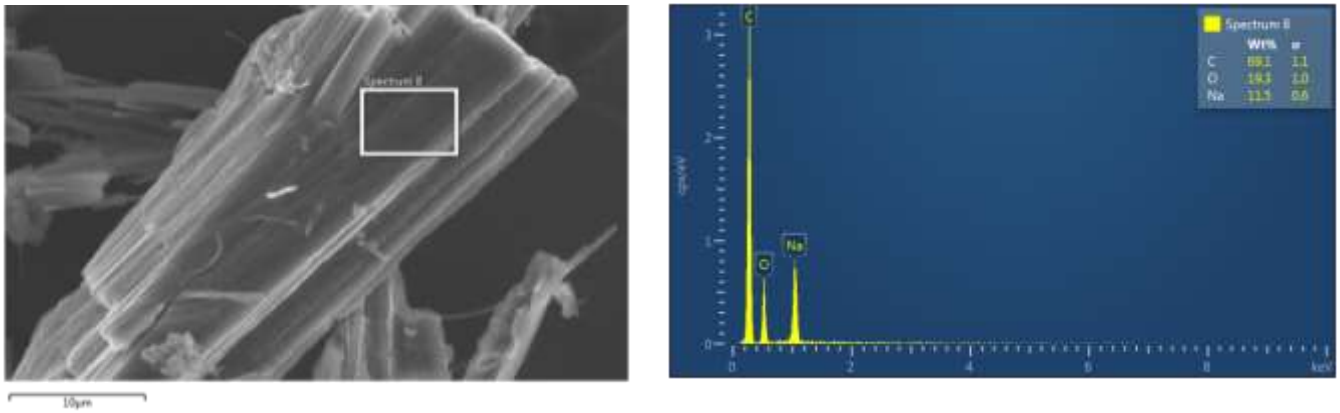

Fig. S7. Energy-dispersive X-ray (EDX) spectrum (right) taken from the identified area in the SEM image (left) of Na(TBAP)(DMF) indicating the primary components of the MOF as being Na, C and O.

2. Ligand (TABPy) synthesis and characterisation

Synthesis of tetraethyl 4,4′,4″,4‴-(pyrene-1,3,6,8-tetrayl)tetrabenzoic acid or H_4TBAPy. Dioxane (250 mL) was degassed with argon for 1 hour. 1,3,6,8-Tetrabromopyrene (4 g, 7.72 mmol), 4-ethoxycarbonylphenylboronic acid (6.6 g, 36.04 mmol), potassium phosphate (13.08 g, 6.16 mmol) and tetrakis(triphenylphosphine)palladium(0) (0.6 g, 0.53 mmol) were added to the dioxane. The reaction mixture was placed under reflux at 90°C and stirred for 72 hours. The reaction mixture was removed from the heat, water (200 mL) was added, and the mixture was allowed to cool to room temperature. A yellow precipitate was collected by filtration and washed with water (200 mL) and acetone (200 mL). The yellow solid was then dried under a constant flow of nitrogen, crushed to a fine powder in a mortar and pestle and added to a solution of boiling chloroform (300 mL). Once the majority of the solid was dissolved the mixture was removed from heat and filtered whilst still hot. The volume of the chloroform solution was reduced by half by blowing nitrogen over it at room temperature. Methanol (300 mL) was then added that resulted in the formation of a yellow precipitate. After standing 2 hours the yellow solid was collected by filtration and dried overnight.

The yellow solid of the ester was added to a solution of dioxane (100 mL). Potassium hydroxide (1.4 g, 25 mmol) was added to water (80 mL) and the aqueous solution was combined with the dioxane solution. The reaction mixture was heated under reflux for 24 hours, allowed to cool and then concentrated HCl was slowly added to until a yellow precipitate formed. The mixture was stirred for another hour and allowed to sit for 3 hours before the yellow solid was filtered and washed with water (200 mL x 3). The yellow solid was dried under a flow nitrogen for 3 hours. The dried solid was then dissolved in boiling DMF and filtered while hot. The DMF solution was allowed to cool and dichloromethane was added until a yellow precipitate formed. The yellow solid was collected by filtration and washed with dichloromethane (100 mL). The product was further dried in under vacuum for 24 hours to afford H_4TBAPy as a pale yellow powder (5.20 g, 85% yield). ^{1}H NMR: 13.09 (s, 4H), 8.20 (s, 4H), 8.17 (d, 8H), 8.07 (s, 2H), 7.86 (d,8H).

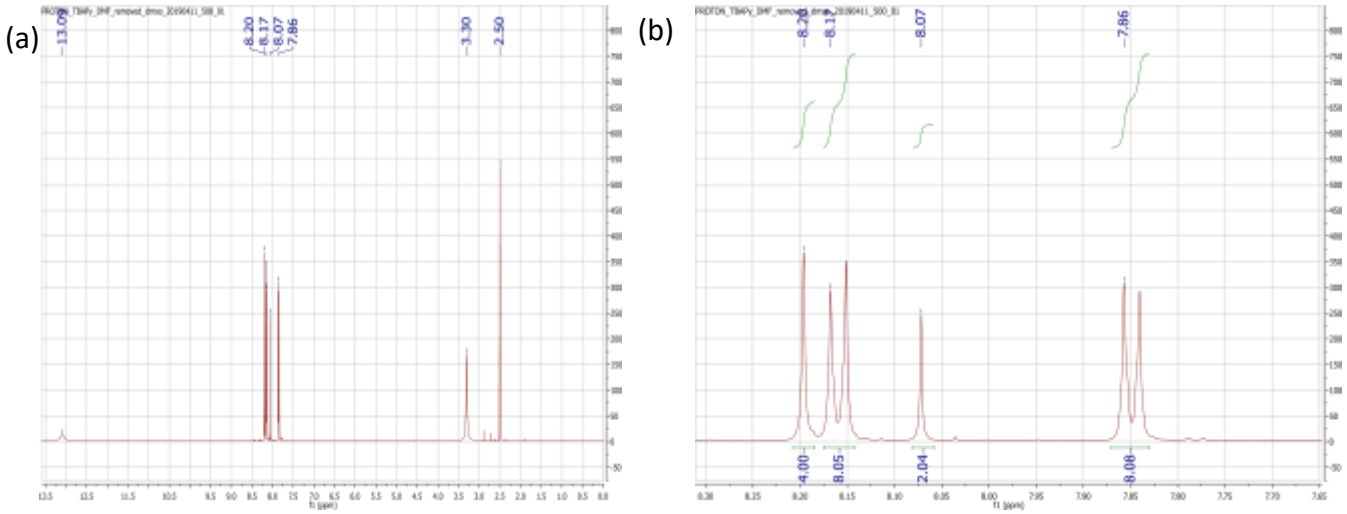

Fig. S8. (a) Full ^{1}H NMR spectrum of TBAPy in DMSO-d_6 (residual solvent at 2.50 ppm and water at 3.30 ppm are indicated). The COOH signal at 13.09 ppm is shown. (b) Enlargement of the aromatic region of the spectrum providing the chemical shift and integration pertaining specifically to TBAPy ligand core and phenyl substituents.

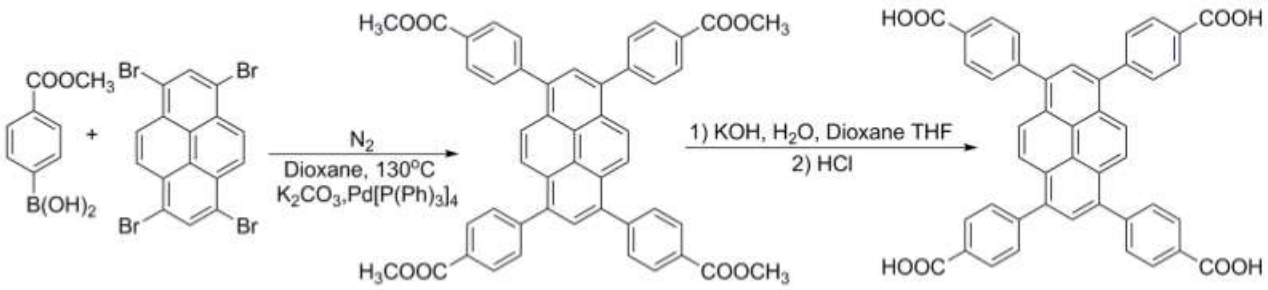

Scheme S1. Procedure used to synthesis TBAPy over two steps from commercially available starting materials.

3. Fitting of time-resolved fluorescence data

Table S1. Multiexponential fitting parameters for the time-resolved fluorescence kinetics of K(TBAPy)(DMF) and Na(TBAPy)(DMF) shown in Figs. 3e and 3f. Uncertainties are expressed as 90% confidence intervals in the fit parameter.

Name	λ (nm)	A_1	τ_1 (ns)	A_2	τ_2 (ns)	A_3	τ_3 (ns)
K(TBAPy)(DMF)	490	0.68 ± 0.02	2.63 ± 0.09	0.32 ± 0.02	9.7 ± 0.3	–	–
	510	0.59 ± 0.02	3.4 ± 0.2	0.41 ± 0.03	11.0 ± 0.4	–	–
	530	0.54 ± 0.01	3.2 ± 0.1	0.46 ± 0.02	11.2 ± 0.2	–	–
	555	0.51 ± 0.02	3.1 ± 0.1	0.49 ± 0.02	11.8 ± 0.2	–	–
Na(TBAPy)(DMF)	490	0.88 ± 0.01	1.02 ± 0.03	0.10 ± 0.01	4.9 ± 0.7	0.02 ± 0.01	16 ± 3
	510	0.73 ± 0.01	1.16 ± 0.04	0.21 ± 0.01	4.9 ± 0.4	0.07 ± 0.01	16 ± 1
	530	0.59 ± 0.01	1.31 ± 0.06	0.28 ± 0.01	5.1 ± 0.4	0.13 ± 0.01	17.0 ± 0.7
	555	0.43 ± 0.03	1.5 ± 0.1	0.36 ± 0.03	5.2 ± 0.5	0.21 ± 0.02	17.7 ± 0.6

4. Additional crystallographic details and structural data

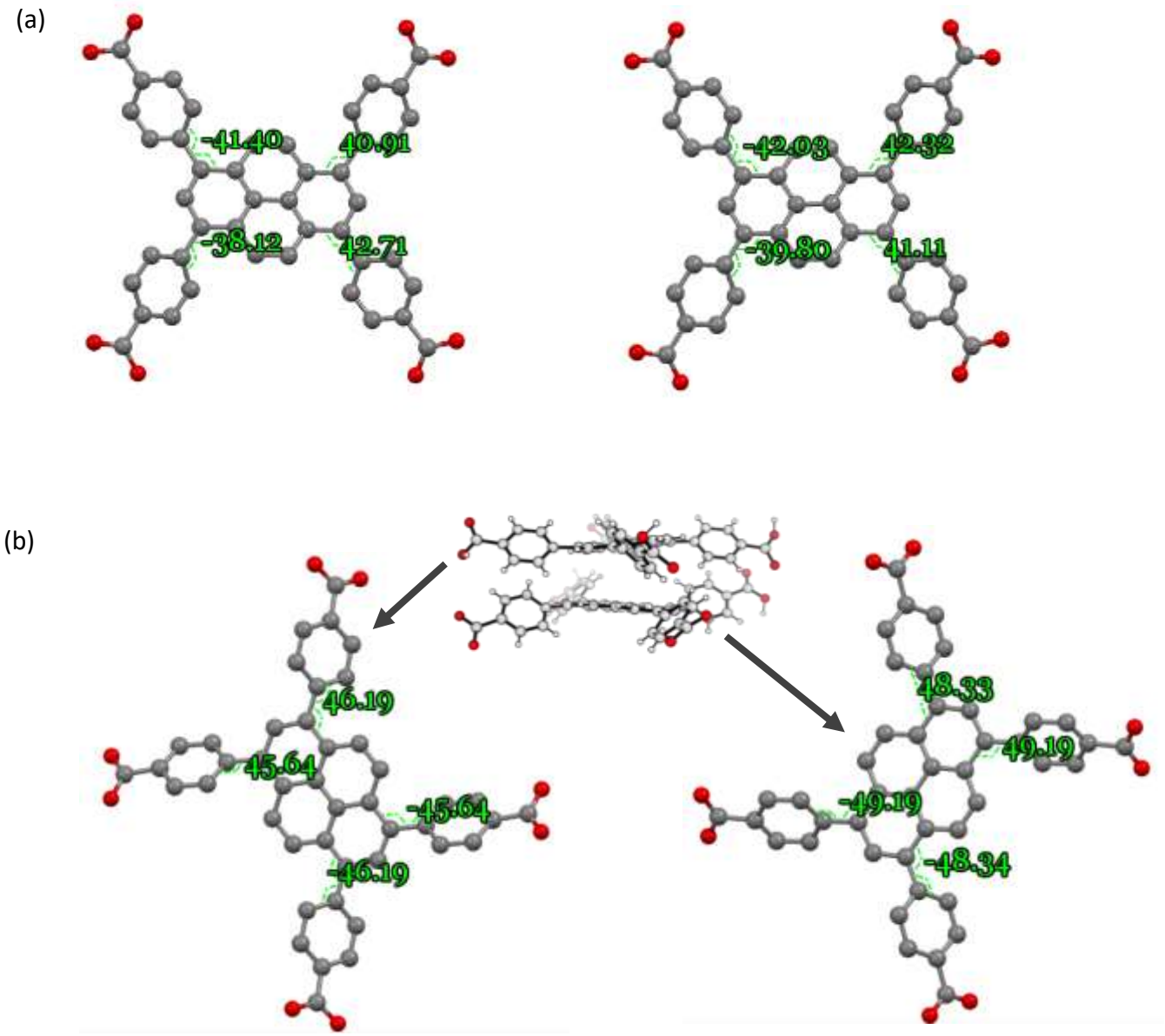

Fig. S9. Pyrene–benzoate dihedral angles (in degrees) for the two structurally distinct ligands contained within each unit cell for (a) K(TBAPy)(DMF) and (b) Na(TBAPy)(DMF).

Fig. S10. Photograph of crystallisation via evaporation of DMF:H_20 (50:50) to give microcrystalline samples of Na(TBAPy)(DMF) (left) and K(TBAPy)(DMF) (right).

Additional refinement details

For Na(TBAPy)(DMF). The crystals of Na(TBAPy)(DMF) were small and poorly diffracting as they are obtained by solvent exchange of a related structure, Na(TBAPy)(acetone), which causes a single crystal-to-single crystal phase change (they could not be obtained directly). The data was omitted above $2\theta = 50^\circ$ to improve the data quality.

For Na(TBAPy)(acetone). There was disorder of the coordinated acetone in the structure and DFIX restraints were used to maintain chemically sensible bond lengths and angles. SIMU and EADP restraints were also used to sensibly refine the acetone molecule.

For K(TBAPy)(DMF). The solvent molecules that coordinate the rod-like SBU in K(TBAPy)(DMF) are heavily disordered, possibly due to a need to accommodate a mixture of DMF, water and a coordinated carbonate anion. DFIX and ISOR restraints were used to refine the most well behaved DMF molecule but the other solvates were truncated to the coordinated oxygen atoms as the data was not of sufficient quality to allow refinement. The formula of the MOF was determined by considering the non-squeezed structure; a mixture of DMF, water and carbonate anion was included in the formula to accurately describe the structure.

Crystallographic information files (cif) have been deposited with the Cambridge Crystallographic Database (CCDC). Deposition numbers 2026823 (Na(TBAPy)(DMF)), 2026825 (Na(TBAPy)(acetone)), and 2026827 (K(TBAPy)(DMF)).

Table S2. Crystal data and structure refinement for Na(TBAPy)(DMF), Na(TBAPy)(acetone), and K(TBAPy)(DMF).

Identification code	Na(TBAPy)(DMF)	Na(TBAPY)(acetone)	K(TBAPy)(DMF)
Empirical formula	$C_{50}H_{36}N_2O_{10}Na_4$	$C_{50}H_{46.5}O_{16.25}Na_4$	$C_{98.25}H_{83.25}N_{3.25}O_{38.5}K_9$
Formula weight	916.77	999.33	2277.33
Temperature/K	150(2)	150(2)	100(2)
Crystal system	monoclinic	monoclinic	monoclinic
Space group	$P2_1/n$	$P2_1/n$	$P2_1/c$
a/Å	21.7180(13)	22.8138(11)	17.329(4)
b/Å	7.8066(6)	7.9496(4)	36.085(7)
c/Å	24.1817(17)	26.0910(11)	15.194(3)
β/°	90.887(6)	96.564(4)	94.59(3)
Volume/Å^3	4099.4(5)	4700.9(4)	9471(3)
Z	4	4	4
ρ_{calc}g/cm^3	1.485	1.412	1.597
μ/mm^{-1}	0.139	0.136	0.505
F(000)	1896.0	2082.0	4698.0
Crystal size/mm^3	0.2 × 0.07 × 0.06	0.4 × 0.1 × 0.1	0.43 × 0.15 × 0.07
Radiation	MoKα (λ = 0.71073)	MoKα (λ = 0.71073)	Synchrotron (λ = 0.71073)
2θ range for data collection/°	6.474 to 50.118	6.746 to 58.722	2.258 to 57.978
Index ranges	-25 ≤ h ≤ 25, -9 ≤ k ≤ 9, -28 ≤ l ≤ 28	-31 ≤ h ≤ 30, -10 ≤ k ≤ 10, -35 ≤ l ≤ 35	-23 ≤ h ≤ 23, -47 ≤ k ≤ 47, -20 ≤ l ≤ 19
Reflections collected	115555	159057	119477
Independent reflections	7259 [R_{int} = 0.3294, R_{sigma} = 0.1651]	12168 [R_{int} = 0.1544, R_{sigma} = 0.1193]	20002 [R_{int} = 0.0282, R_{sigma} = 0.0175]
Data/restraints/parameters	7259/0/599	12168/34/690	20002/16/1205
Goodness-of-fit on F^2	1.119	1.029	1.053
Final R indexes [I>=2σ (I)]	R_1 = 0.1321, wR_2 = 0.3476	R_1 = 0.0698, wR_2 = 0.1399	R_1 = 0.0722, wR_2 = 0.2254
Final R indexes [all data]	R_1 = 0.2167, wR_2 = 0.3874	R_1 = 0.1475, wR_2 = 0.1690	R_1 = 0.0829, wR_2 = 0.2364
Largest diff. peak/hole / e Å^{-3}	0.72/-0.47	0.43/-0.38	1.92/-0.53

5. Preparation of LED device

A glass indium-tin oxide (ITO) substrate was cleaned using isopropanol and distilled water then dried thoroughly. 50 mg of Na(TBAPy)(DMF) was ground into a fine powder and added to 20 mL of acetone to create a suspension. The suspension was spin-coated (4000 rpm for 30 secs) on to the conductive side of the glass substrate. Several MOF layers were added (10–15) until an even coating had been achieved. Next, a single layer of light-emitting copolymer poly[(9,9-dioctyl-2,7divinylenefluorenylene)-alt-co-(2-methoxy-5-(2-ethylhexyloxy)-1,4-phenylene)] (PFO-co-MEH-PPV), which had been pre-dissolved in di-chloromethane at a concentration of 10 mg/mL, was added using the same spin coating process. Once dried, a cotton swab dipped in chloroform was used to expose the ITO on one of the corners of the glass substrate. The exposed corner was connected the negative terminal of a power source and a gallium/in-dium eutectic was used to connect the light-emitting layer to the positive terminal (see Fig. S11).

(a) (b) (c)

Fig. S11. (a) Schematic of light-emitting diode fabricated using Na(TBAPy)(DMF) as a hole transport layer, (b) photograph of coated substrate connected to a DC power source and (c) photograph of active LED emitting light at 4.45 V (26 mA).

6. Density functional theory (DFT) calculations

Density functional theory (DFT) with the ωB97X-D exchange–correlation functional[1] was selected as the computational method as it has been shown to be a good compromise between accuracy and computational expense for a wide range of molecules. ωB97X-D is considered one of the best functionals in terms of overall accuracy for a broad range of chemical properties and molecules,[2] it has been found to be one of the most accurate functionals for excited-state geometries of a range of organic molecules,[3] and it has consistently been found to be one of the most accurate functionals in benchmarks of time-dependent DFT (TD-DFT) calculations of excited-state properties.[4] Importantly for this study, the ωB97X-D functional corrects for spurious self-interaction errors by separating the Coulomb interaction into short- and long-range parts with the long-range part treated using Hartree–Fock exchange, allowing accurate treatment of non-local phenomena such as electron delocalization and charge-transfer excitations, which common hybrid functionals such as B3LYP fail to describe; it also contains a dispersion correction that allows accurate treatment of molecular packing due to weak van der Waals interactions. ωB97X-D has been strongly recommended for calculations on organic molecules with extended π conjugation (such as pyrene).[5] ωB97X-D has previously been combined with the basis sets (6-31G* and 6-31+G*) used in this study to accurately calculate optical absorption spectra and charge-carrier mobilities of similar organic π-conjugated systems.[6] Such results give confidence in the accuracy of the calculations for the systems in this study.

For each MOF, DFT calculations were performed using Q-Chem version 5.1.1[7] on a fragment comprising TBAPy ligands extracted from the experimental X-ray crystal structure (in each case, the closest ligand pair in the framework was chosen). To mimic the geometric constraints in the MOF framework, the carboxylate carbon and oxygen atoms in the ligands were fixed at their positions in the experimental crystal structure during geometry optimizations. For calculations of an isolated TBAPy ligand, no geometric constraints were applied. In all case, each carboxylate group in the TBAPy ligands was terminated by H^+ to enforce charge neutrality in the neutral systems and a +1 charge in the cationic systems used for the charge-transfer calculations. Geometry optimizations in the ground state were initiated from the experimental crystal structure, while optimizations of excited states and charge-localized states were initiated from the optimized ground-state geometry.

To calculate the electronic absorption spectrum of each system, the 30 lowest energy singlet transitions were computed in the ground-state (S_0) geometry. Since Kasha's rule dictates that emission occurs only from the lowest excited state, the electronic emission spectrum was calculated from the lowest energy singlet transition computed in the geometry of the first (S_1) excited singlet state.

To calculate the rate constant for hole transfer between the TBAPy ligands in each MOF dimer, the geometry was optimized with the net +1 charge of the system constrained to one of the ligands using CDFT. The electronic coupling V_{da} between diabatic states in which the +1 charge is localised on one or the other ligand and the reorganization energy λ was calculated using CDFT-CI, with the V_{da} given by either off-diagonal element and λ given by the difference between the diagonal elements of the CDFT-CI Hamiltonian matrix the orthogonalized basis. As such, the calculated reorganisation energy only includes the inner-sphere component due to relaxation of the molecules directly involved in the charge transfer and excludes the outer-sphere component due to relaxation of the environment, but the latter contribution is expected to be small compared with the inner-sphere component in a rigid MOF framework. This level of approximation is also expected to be sufficient for comparison of relative hole-transfer rates for the different MOFs. The hole-transfer rate constant k_h was calculated with Marcus electron-transfer theory using[8]

$$k_{\mathrm{h}} = \frac{2\pi}{\hbar}|V_{\mathrm{da}}|^2\sqrt{\frac{1}{4\pi k_{\mathrm{B}}T\lambda}}\exp\left[-\frac{(\Delta G^{\circ}+\lambda)^2}{4\lambda k_{\mathrm{B}}T}\right] \quad (1)$$

where the free-energy change ΔG° for the hole transfer process is zero because the donor and acceptor ligands are identical.

Most calculations used default values of parameters in Q-Chem version 5.1.1, but to obtain SCF convergence in calculations using the 6-31+G* basis set, BASIS_LIN_DEP_THRESH (which sets the threshold for determining linear dependence in the basis set) was set to 5 to reduce the threshold for linear dependence, XC_GRID (which specifies the type of grid to use in DFT calculations) was set to 3 to increase the number of grid points, and THRESH (which sets the cutoff for neglect of two electron integrals) was set to 12 (or 14 for CDFT-CI calculations) to reduce the threshold.

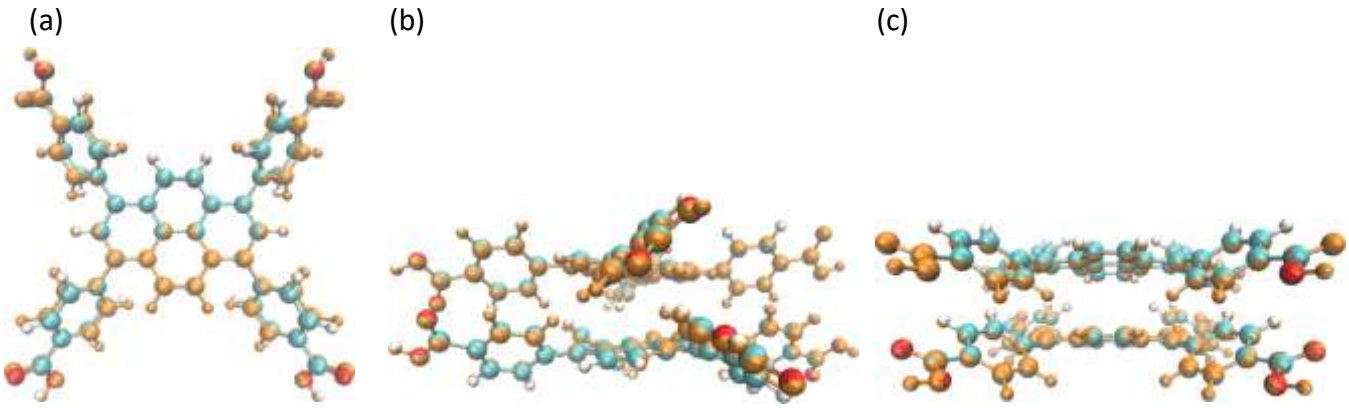

Fig. S12. Overlay of optimised ground-state (S0) and lowest energy excited-state (S1) structures (with atoms in excited-state structures in orange) for (a) TBAPy monomer, (b) Na(TBAPy)(DMF) MOF dimer, and (c) K(TBAPy)(DMF) MOF dimer. The most significant change in the geometry of the TBAPy monomer is the reduction in the pyrene – benzoate dihedral angle by an average of 12.1° (from 57.2° to 45.1°) from the S_0 to S_1 structures. The MOF dimers hardly change between the S_0 and S_1 structures due to the geometric constraints on the positions of carboxyl atoms, with the corresponding dihedral decreasing on average by 1.7° (from 47.4° to 45.6°) and 1.9° (from 42.1° to 40.2°) for Na(TBAPy)(DMF) and K(TBAPy)(DMF), respectively. The calculated dihedral angles are the same ones as shown in Fig. S9 and show reasonable agreement with experiment for the S_0 structures.

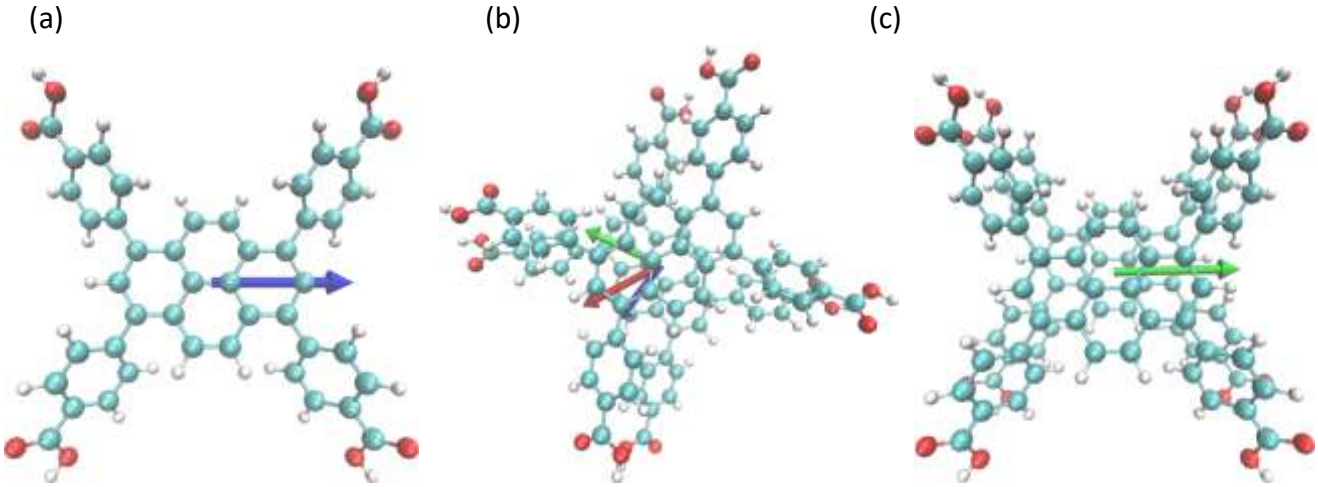

Fig. S13. Calculated transition dipole moments (TDMs) for (a) TBAPy monomer, (b) Na(TBAPy)(DMF) MOF dimer, and (c) K(TBAPy)(DMF) MOF dimer. The TDM for the $S_0 \rightarrow S_1$ and $S_0 \rightarrow S_2$ transitions in the S_0 geometry are in blue and green, respectively, and that for the $S_0 \rightarrow S_1$ transition in the S_1 geometry is shown in red. Only the $S_0 \rightarrow S_1$ transitions in the S_0 geometry is shown in (a) and only the $S_0 \rightarrow S_2$ transitions in the S_0 geometry in (c), since the $S_0 \rightarrow S_1$ transition has negligible TDM for K(TBAPy)(DMF) and the TDMs do not change direction noticeably in the S_1 geometry for the TBAPy monomer or K(TBAPy)(DMF) MOF dimer. In both (b) and (c), the TDMs shown are aligned in the plane of the stacked pyrene cores.

Charge-transfer rate constants

Table S3. Calculated electronic couplings, reorganisation energies, and hole-transfer rate constants for MOF TBAPy dimers.

MOF	electronic coupling V_{da} (meV)	reorganisation energy λ (meV)	hole transfer rate constant k_h (s^{-1})
Na(TBAPy)(DMF)	45.6	256	5.7×10^{12}
K(TBAPy)(DMF)	19.8	230	1.5×10^{12}
NU-1000	3.6	262	3.3×10^{10}

The calculated electronic coupling and reorganisation energy for NU-1000 are comparable (2.7 and 280 meV, respectively) to those calculated previously by Patwardhan and Schatz[9] for the same ligand dimer in NU-1000 but using a different density functional, basis set, and charge-transfer calculation method to that used here.

7. References

1 J.-D. Chai and M. Head-Gordon, *Phys. Chem. Chem. Phys.*, 2008, **10**, 6615–6620.

2. N. Mardirossian, M. Head-Gordon, *Mol. Phys.* 2017, **19**, 2315–2372.

3. E. Bremond, M. Savarese, C Adamo, and D. Jacquemin, *J. Chem. Theory Comput.* 2018, **14**, 3715–3727.

4. A. D. Laurent and D. Jacquemin, *Int. J. Quant. Chem.*, 2013, **113**, 2019–2039.

5. K. Do, M. K. Ravva, T. Wang, and J.-L. Bredas, *Chem. Mater.* 2017, **29**, 346–354.

6. J. T. Ly, E. K. Burnett, S. Thomas, A. Aljarb, Y. Liu, S. Park, S. Rosa, Y. Yi, H. Lee, T. Emrick, T. P. Russell, J.-Luc Brédas, and A. L. Briseno, *ACS Appl. Mater. Interfaces*, 2018, **10**, 40070–40077.

7. Y. Shao, Z. Gan, E. Epifanovsky, A. T. B. Gilbert, M. Wormit, J. Kussmann, A. W. Lange, A. Behn, J. Deng, X. Feng, D. Ghosh, M. Goldey, P. R. Horn, L. D. Jacobson, I. Kaliman, R. Z. Khaliullin, T. Kuš, A. Landau, J. Liu, E. I. Proynov, Y. M. Rhee, R. M. Richard, M. A. Rohrdanz, R. P. Steele, E. J. Sundstrom, H. L. Woodcock, P. M. Zimmerman, D. Zuev, B. Albrecht, E. Alguire, B. Austin, G. J. O. Beran, Y. A. Bernard, E. Berquist, K. Brandhorst, K. B. Bravaya, S. T. Brown, D. Casanova, C. M. Chang, Y. Chen, S. H. Chien, K. D. Closser, D. L. Crittenden, M. Diedenhofen, R. A. Distasio, H. Do, A. D. Dutoi, R. G. Edgar, S. Fatehi, L. Fusti-Molnar, A. Ghysels, A. Golubeva-Zadorozhnaya, J. Gomes, M. W. D. Hanson-Heine, P. H. P. Harbach, A. W. Hauser, E. G. Hohenstein, Z. C. Holden, T. C. Jagau, H. Ji, B. Kaduk, K. Khistyaev, J. Kim, J. Kim, R. A. King, P. Klunzinger, D. Kosenkov, T. Kowalczyk, C. M. Krauter, K. U. Lao, A. D. Laurent, K. V. Lawler, S. V. Levchenko, C. Y. Lin, F. Liu, E. Livshits, R. C. Lochan, A. Luenser, P. Manohar, S. F. Manzer, S. P. Mao, N. Mardirossian, A. V. Marenich, S. A. Maurer, N. J. Mayhall, E. Neuscamman, C. M. Oana, R. Olivares-Amaya, D. P. Oneill, J. A. Parkhill, T. M. Perrine, R. Peverati, A. Prociuk, D. R. Rehn, E. Rosta, N. J. Russ, S. M. Sharada, S. Sharma, D. W. Small, A. Sodt, T. Stein, D. Stück, Y. C. Su, A. J. W. Thom, T. Tsuchimochi, V. Vanovschi, L. Vogt, O. Vydrov, T. Wang, M. A. Watson, J. Wenzel, A. White, C. F. Williams, J. Yang, S. Yeganeh, S. R. Yost, Z. Q. You, I. Y. Zhang, X. Zhang, Y. Zhao, B. R. Brooks, G. K. L. Chan, D. M. Chipman, C. J. Cramer, W. A. Goddard, M. S. Gordon, W. J. Hehre, A. Klamt, H. F. Schaefer, M. W. Schmidt, C. D. Sherrill, D. G. Truhlar, A. Warshel, X. Xu, A. Aspuru-Guzik, R. Baer, A. T. Bell, N. A. Besley, J. Da Chai, A. Dreuw, B. D. Dunietz, T. R. Furlani, S. R. Gwaltney, C. P. Hsu, Y. Jung, J. Kong, D. S. Lambrecht, W. Liang, C. Ochsenfeld, V. A. Rassolov, L. V. Slipchenko, J. E. Subotnik, T. Van Voorhis, J. M. Herbert, A. I. Krylov, P. M. W. Gill and M. Head-Gordon, *Mol. Phys.*, 2015, **113**, 184–215.

8. R. A. Marcus, *Annu. Rev. Phys. Chem.*, 1964, **15**, 155-196.

9. S. Patwardhan and G. C. Schatz, *J. Phys. Chem. C*, 2015, **119**, 24238–24247.